Supporting Information

Highly Porous Metal-organic Framework Glass Design and Application for Gas Separation Membranes

Shichun Li[1]*†, Chao Ma[2]†, Jingwei Hou[3,4] , Shuwen Yu[3,4,5], Aibing Chen[6], Juan Du[6], Philip A. Chater[7], Dean S. Keeble[7], Zhihua Qiao[2]*, Chongli Zhong[2], David A. Keen[8], Yu Liu[1], Thomas D. Bennett[9]*

Affiliations:

[1] Institute of Chemical Materials, China Academy of Engineering Physics, Mianyang, 621900, China.

[2] State Key Laboratory of Separation Membranes and Membrane Processes, Tiangong University, Tianjin, 300387, China.

[3] School of Chemical Engineering, The University of Queensland, St Lucia, QLD 4072, Australia.

[4] ARC Centre of Excellence for Green Electrochemical Transformation of Carbon Dioxide, Brisbane, Australia

[5] School of Chemistry and Chemical Engineering, Suzhou University, Suzhou, 234000, China.

[6] College of Chemical and Pharmaceutical Engineering, Hebei University of Science and Technology, Shijiazhuang, 050018, China.

[7] Diamond Light Source Ltd, Diamond House, Harwell Science & Innovation Campus, Didcot, Oxfordshire, OX11 0DE, UK.

[8] ISIS Facility, Rutherford Appleton Laboratory, Harwell Campus, Didcot, Oxon OX11 0QX, UK.

[9] Department of Materials Science and Metallurgy, University of Cambridge, Cambridge, CB3 0FS, UK.

* Corresponding authors: lishichun@caep.cn (S.L.); qiaozhihua@tiangong.edu.cn (Z.Q.); tdb35@cam.ac.uk (T.D.B.)

† These authors contributed equally to this work.

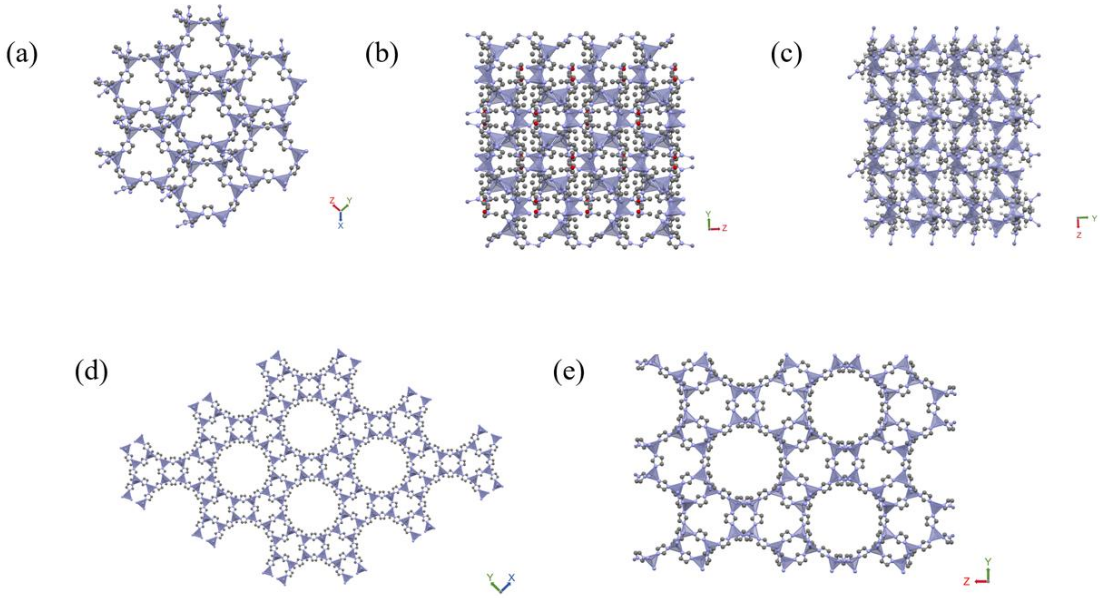

Supplementary Fig. 1 ZIF structure diagrams (a) ZIF-8, (b) ZIF-62, (c) ZIF-4, (d) AFI-[$Zn(Im)_2$], and (e) CAN-[$Zn(Im)_2$][S1-S6]. The deep purple triangle represents Zn atoms, the purple sphere represents N atoms, and the gray sphere represents C atoms.

Supplementary Table 1. Lists of representative ZIFs and their textural properties

Topology	**Materials**	**Framework formula**	**Apertures Å**	**Ref.**
SOD	ZIF-8	$Zn(mIm)_2$	3.4	S2
CAG	ZIF-62	$Zn(Im)_{1.75}(bIm)_{0.25}$	1.4	S3, S4
CAG	ZIF-4	$Zn(Im)_2$	2.0	S5
AFI	AFI-$Zn(Im)_2$	$Zn(Im)_2$	20.0	S6
CAN	CAN-$Zn(Im)_2$	$Zn(Im)_2$	17.1	S6

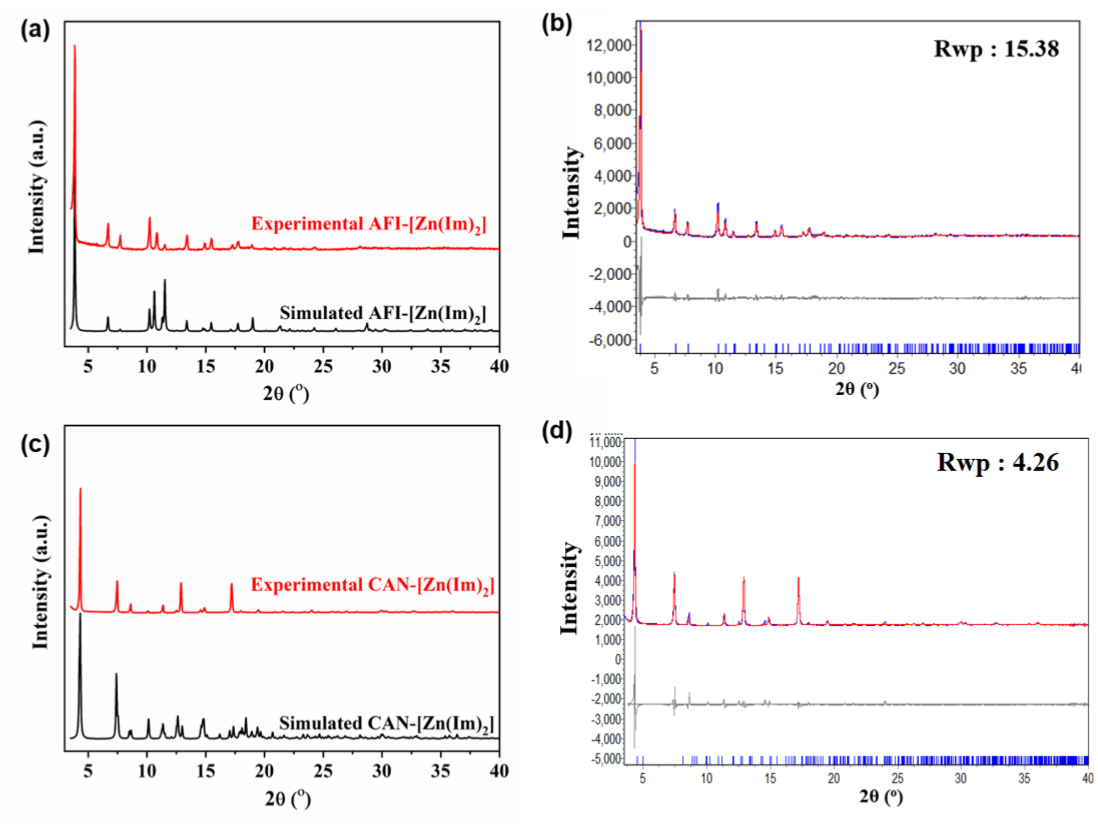

Supplementary Fig. 2 XRD patterns and Powley refinement results of (a-b) AFI-[Zn(Im)$_2$] and (c-d) CAN-[Zn(Im)$_2$]. The simulated XRD patterns were calculated from reported cif files. The 'a.u.' represents 'arbitrary units'.

Supplementary Table 2 Lattice parameters of AFI-[Zn(Im)$_2$] and CAN-[Zn(Im)$_2$] obtained from reported cif files and Pawley refinement.

	Space group	**a (Å)**	**b (Å)**	**c (Å)**	**α (º)**	**β (º)**	**γ (º)**	**Ref.**
AFI-[Zn(Im)$_2$]	P6/MCC	26.4372	26.4372	16.6315	90	90	120	Cif
AFI-[Zn(Im)$_2$]	P6/MCC	26.284(7)	26.284(7)	16.243(6)	90	90	120	This work
CAN-[Zn(Im)$_2$]	Pnma	9.6256(8)	23.436(2)	41.593(3)	90	90	90	Cif
CAN-[Zn(Im)$_2$]	Pnma	9.927(4)	19.839(7)	39.00(1)	90	90	90	This work

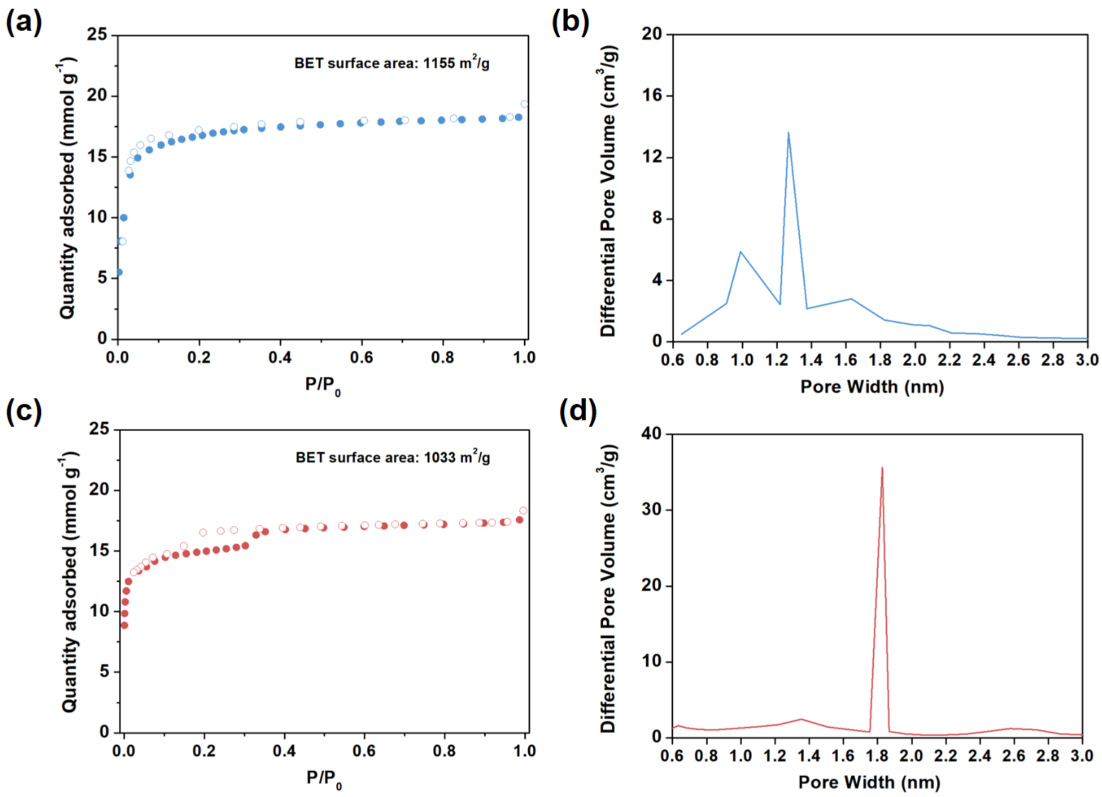

Supplementary Fig. 3 N_2 isotherms and pore distribution of (a-b) AFI-[Zn(Im)$_2$] and (c-d) CAN-[Zn(Im)$_2$]. The filled and hollow circles represent adsorption and desorption, respectively.

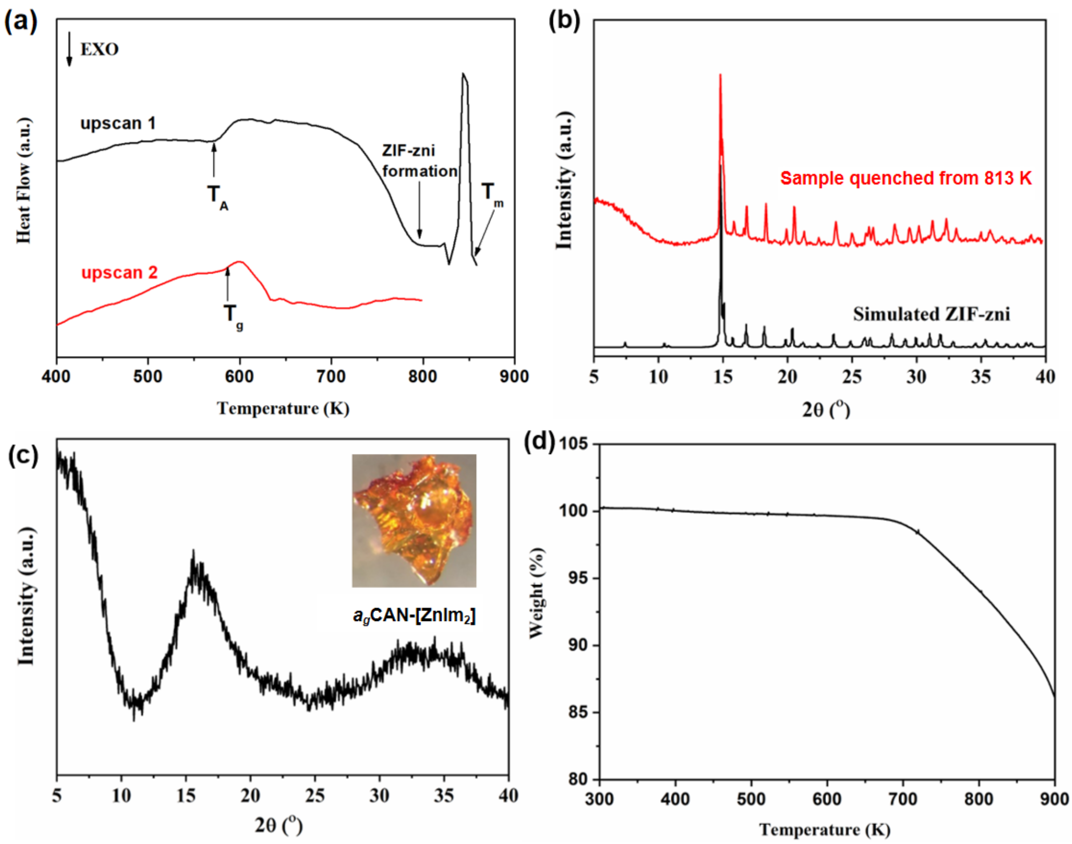

Supplementary Fig. 4 Melting behaviours of AFI-[Zn(Im)$_2$]. (a) Enthalpic responses of AFI-[Zn(Im)$_2$] on both the first (black) DSC heating upscan at 20 K/min and the second (red) one at 10 K/min under Ar. (b) XRD patterns of the sample quanched from 813 K and calculated from the reported cif file of ZIF-zni. (c) XRD patterns of a_gAFI-[Zn(Im)$_2$], and the insert is a photograph of a_gAFI-[Zn(Im)$_2$]. (d) TGA curve of AFI-[Zn(Im)$_2$] measured under Ar. The 'a.u.' represents 'arbitrary units'.

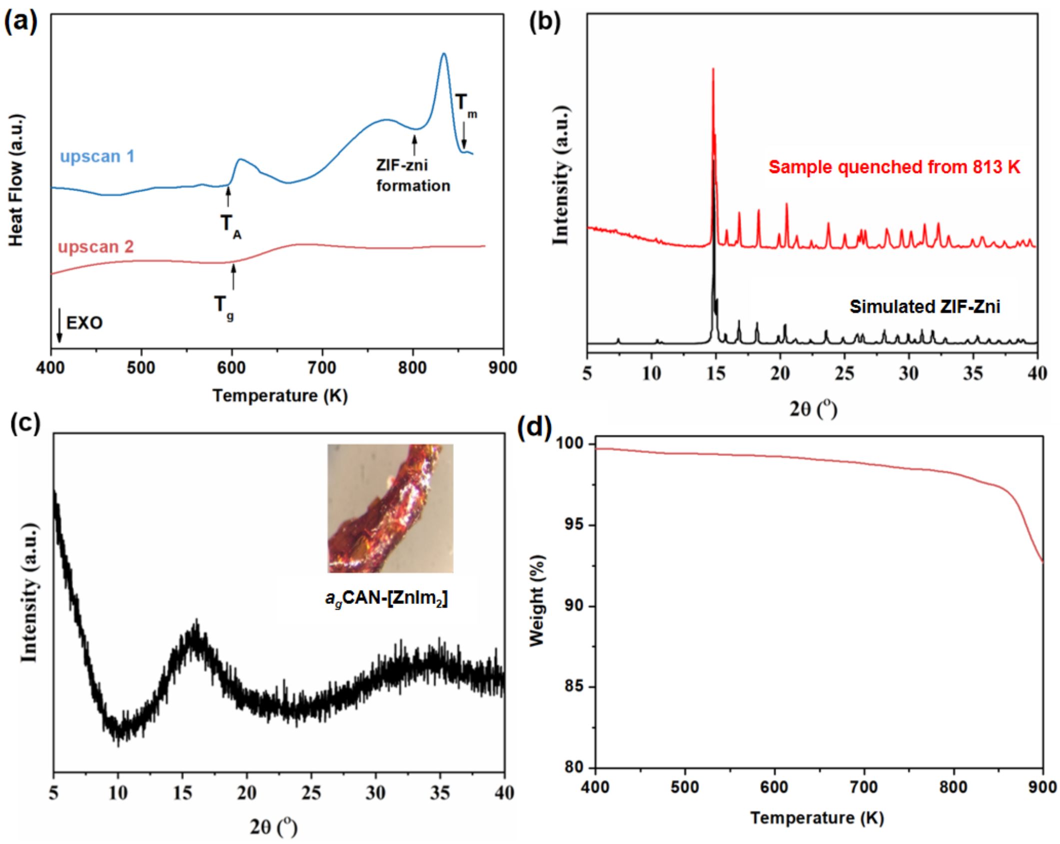

Supplementary Fig. 5 Melting behaviours of CAN-[Zn(Im)$_2$]. (a) Enthalpic responses of CAN-[Zn(Im)$_2$] under Ar. (b) XRD patterns of the sample quenched from 813 K and calculated from the reported cif file of ZIF-zni. (c) XRD patterns of a_gCAN-[Zn(Im)$_2$], and the insert is a photograph of a_gCAN-[Zn(Im)$_2$]. (d) TGA curve of CAN-[Zn(Im)$_2$] measured under Ar. The ‘a.u.’ represents ‘arbitrary units’.

Supplementary Table 3. Summary of the temperature values obtained from the DSC data.

Material	Composition	T_m (K)	T_g (K)	T_A (K)
AFI-bIm	$Zn(Im)_{1.68}(bIm)_{0.32}$	705	607	618
CAN-bIm	$Zn(Im)_{1.73}(bIm)_{0.27}$	670	591	595
AFI-Im	$Zn(Im)_2$	853	588	573
CAN-Im	$Zn(Im)_2$	853	600	598

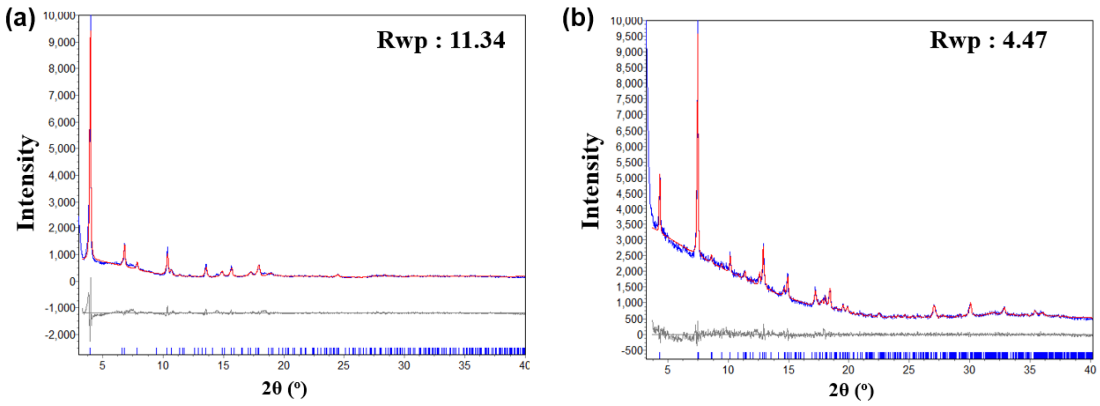

Supplementary Fig. 6 Powley refinement results of (a) AFI-[Zn(Im)$_{1.68}$(bIm)$_{0.32}$] and (b) CAN-[Zn(Im)$_{1.73}$(bIm)$_{0.27}$].

Supplementary Table 4 Lattice parameters of MOFs obtained from reported cif files and Pawley refinement.

	Space group	a (Å)	b (Å)	c (Å)	α (°)	β (°)	γ (°)	Ref.
AFI-[Zn(Im)$_2$]	P6/MCC	26.4372	26.4372	16.6315	90	90	120	Cif
AFI-[Zn(Im)$_{1.68}$(bIm)$_{0.32}$]	P6/MCC	26.137(8)	26.137(8)	16.59(1)	90	90	120	This work
CAN-[Zn(Im)$_2$]	Pnma	9.6256(8)	23.436(2)	41.593(3)	90	90	90	Cif
CAN-[Zn(Im)$_{1.73}$(bIm)$_{0.27}$]	Pnma	9.623(3)	23.54(1)	41.21(1)	90	90	90	This work

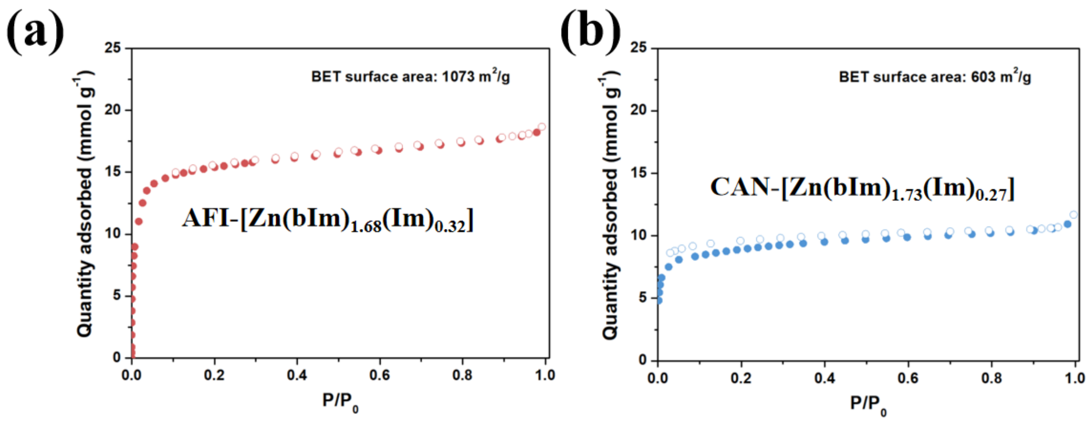

Supplementary Fig. 7 N_2 isotherms of (a) AFI-[Zn(Im)$_{1.68}$(bIm)$_{0.32}$] and (b) CAN-[Zn(Im)$_{1.73}$(bIm)$_{0.27}$].

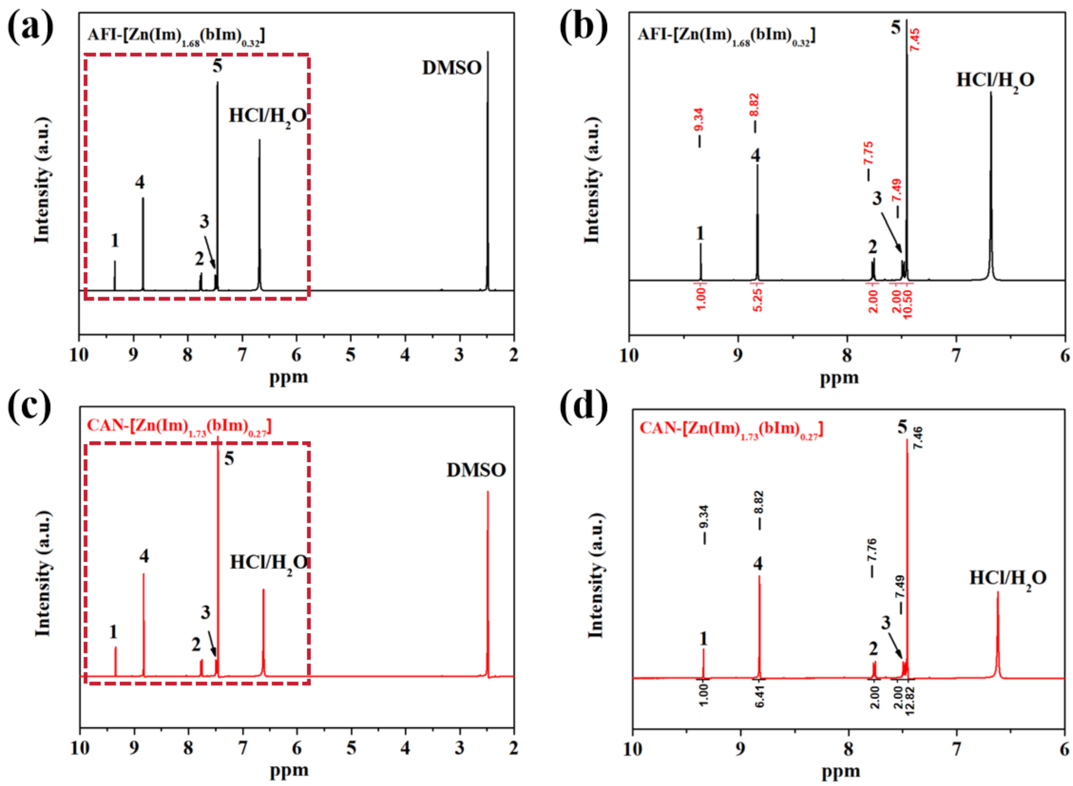

Supplementary Fig. 8 ^{1}H NMR and enlarged aromatic region for (a, b) AFI-[Zn(Im)$_{1.68}$(bIm)$_{0.32}$] and (c, d) CAN-[Zn(Im)$_{1.73}$(bIm)$_{0.27}$]. The ‘a.u.’ represents ‘arbitrary units’.

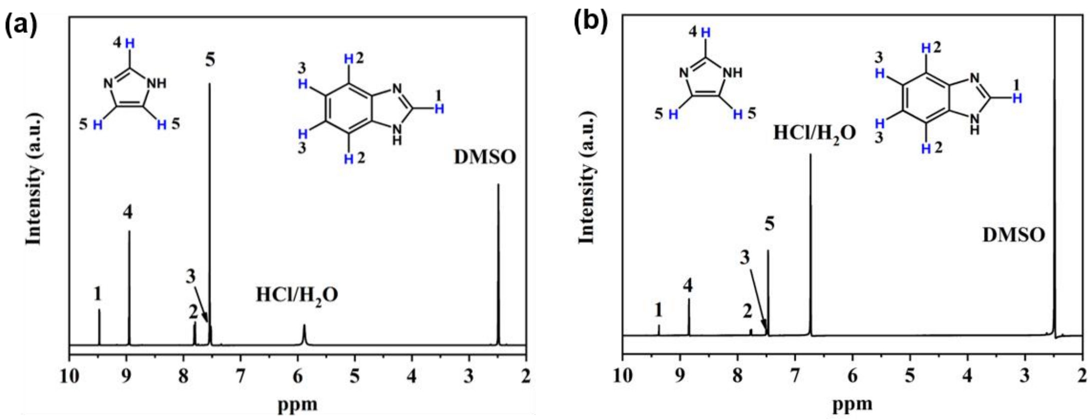

Supplementary Fig. 9 ^{1}H NMR results of (a) a_gAFI-[$Zn(Im)_{1.68}(bIm)_{0.32}$] and (b) a_gCAN- [$Zn(Im)_{1.55}(bIm)_{0.45}$]. The ‘a.u.’ represents ‘arbitrary units’.

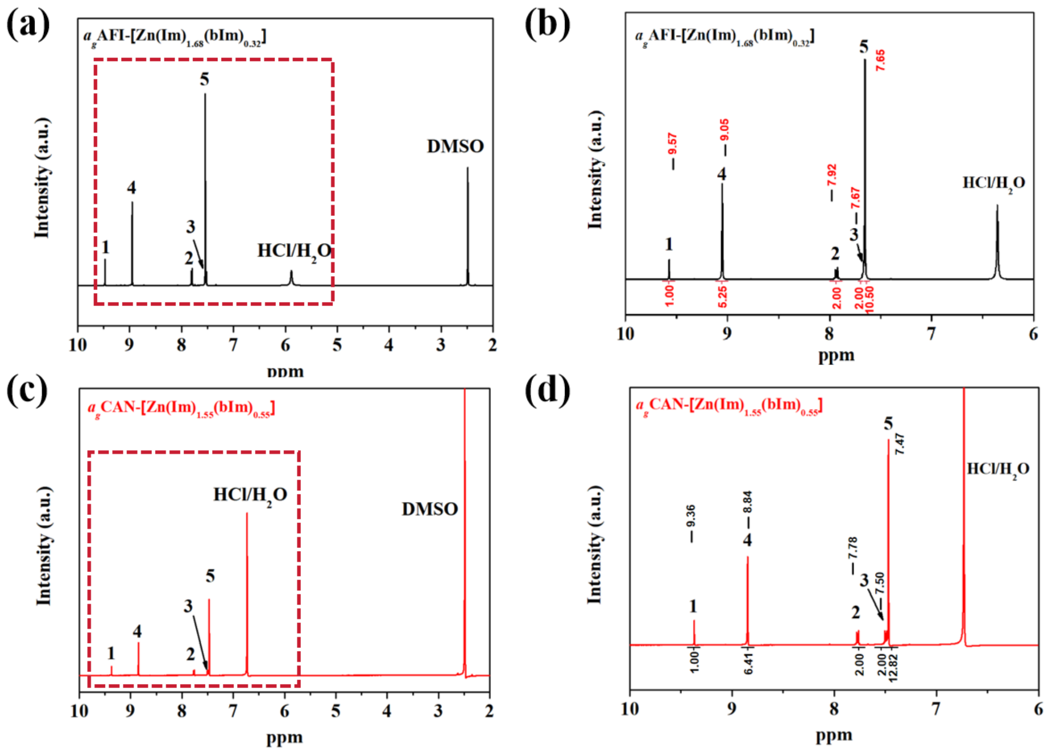

Supplementary Fig. 10 ^{1}H NMR and Enlarged aromatic region for (a, b) a_gAFI-[Zn(Im)$_{1.68}$(bIm)$_{0.32}$] and (c, d) a_gCAN-[Zn(Im)$_{1.55}$(bIm)$_{0.55}$]. The ‘a.u.’ represents ‘arbitrary units’.

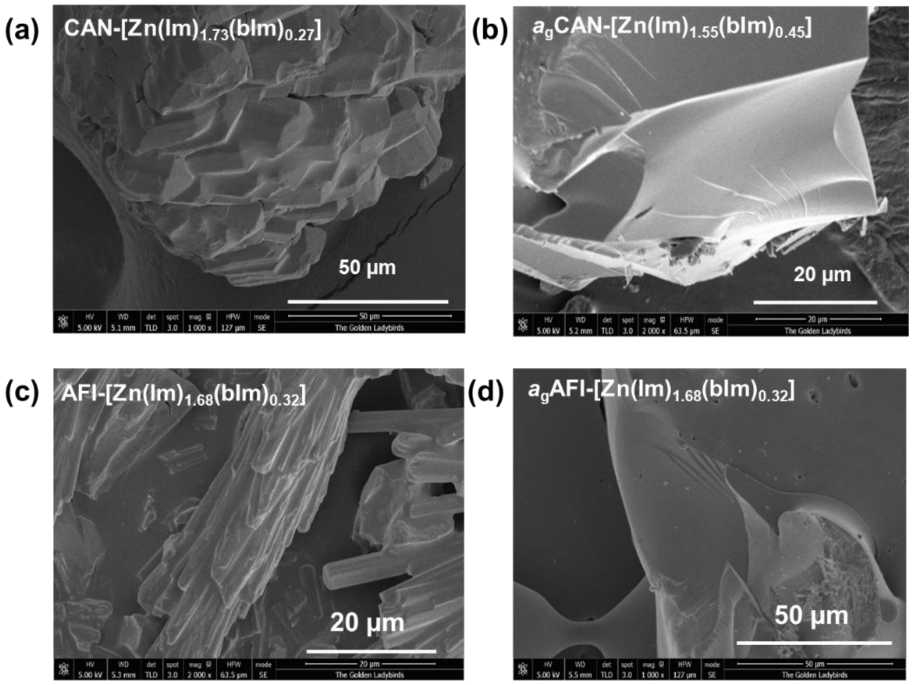

Supplementary Fig. 11 SEM images of (a) CAN-[$Zn(Im)_{1.73}(bIm)_{0.27}$], (b) a_gCAN-[$Zn(Im)_{1.55}(bIm)_{0.45}$], (c) AFI-[$Zn(Im)_{1.68}(bIm)_{0.32}$] and (d) a_gAFI-[$Zn(Im)_{1.68}(bIm)_{0.32}$].

Supplementary Table 5. Summary of the phase transition enthalpies obtained from the DSC data.

Material	**Composition**	***T_m*** **(K)**	***T_g*** **(K)**	***ΔH_m*** **(KJ/mol)**	**Ref.**
ZIF-62	$Zn(Im)_{1.75}(bIm)_{0.25}$	708	604	2.92	S7
ZIF-4	$Zn(Im)_2$	852	-	11.46	S8
TIF-4	$Zn(Im)_{1.68}(mbIm)_{0.32}$	709	611	2.69	S8
ZIF-zni	$Zn(Im)_2$	858	-	11.88	S8
ZIF-UC-5	$Zn(Im)_{1.62}(ClbIm)_{0.38}$	701	-	-	S9
ZIF-8-$mIm_{0.15}Im_{0.74}bIm_{0.11}$	$Zn(mIm)_{0.15}(Im)_{0.74}(bIm)_{0.11}$	641	-	0.66	S10
AFI	$Zn(Im)_{1.68}(bIm)_{0.32}$	705	607	0.52	This work
CAN	$Zn(Im)_{1.73}(bIm)_{0.27}$	670	591	0.50	This work

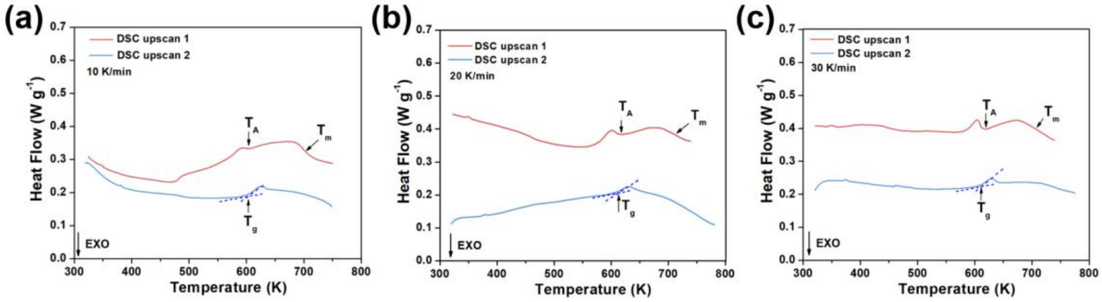

Supplementary Fig. 12 DSC curves of AFI-[Zn(Im)$_{1.68}$(bIm)$_{0.32}$] at varying heating rates (a) 10 K, (b) 20 K, and (c) 30 K.

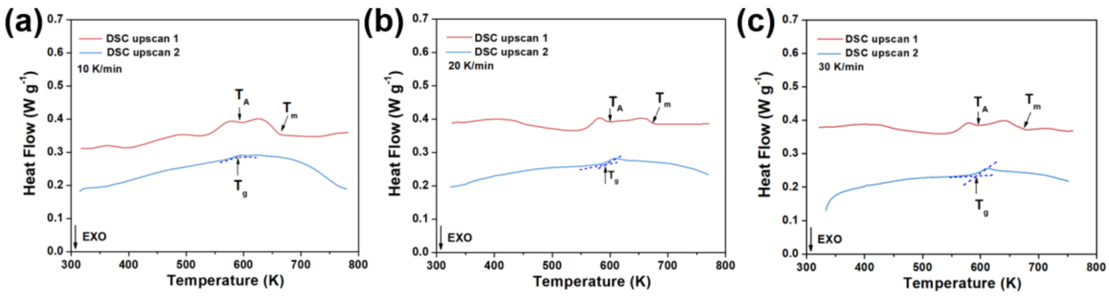

Supplementary Fig. 13 DSC curves of CAN-[Zn(Im)$_{1.73}$(bIm)$_{0.27}$] at varying heating rates (a) 10 K, (b) 20 K, and (c) 30 K.

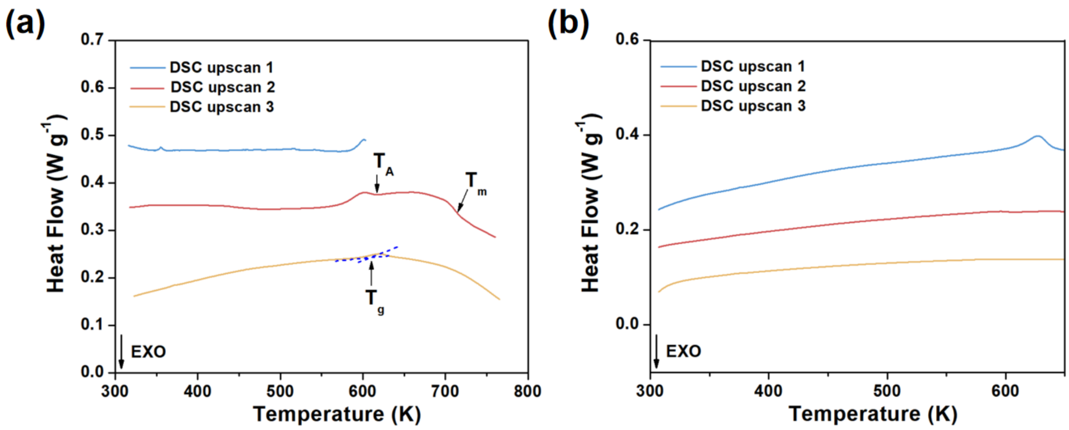

Supplementary Fig. 14. DSC curves of AFI-[$Zn(Im)_{1.68}(bIm)_{0.32}$]. (a) heat up to T_A for the first scan, (b) heat up to above T_A for all three scans.

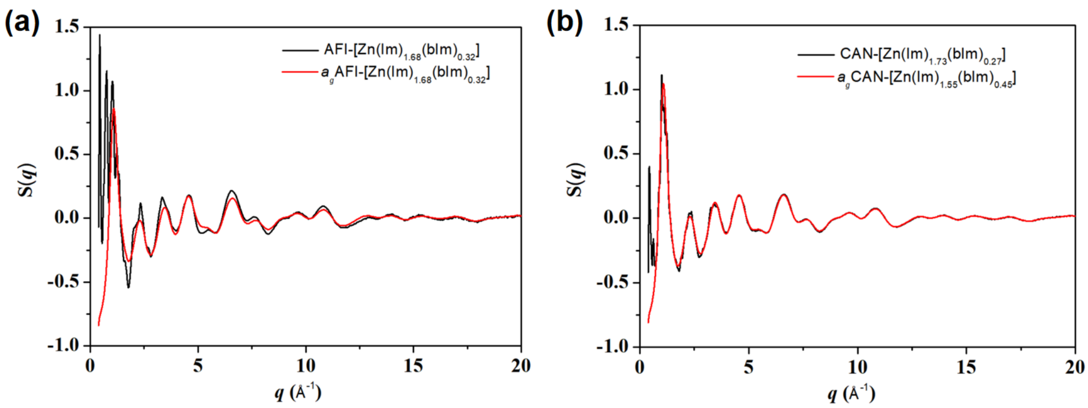

Supplementary Fig. 15 Structure factors, $S(q)$, of (a) AFI-[Zn(Im)$_{1.68}$(bIm)$_{0.32}$] and a_gAFI-[Zn(Im)$_{1.68}$(bIm)$_{0.32}$], and (b) CAN-[Zn(Im)$_{1.73}$(bIm)$_{0.27}$] and a_gCAN-[Zn(Im)$_{1.55}$(bIm)$_{0.45}$].

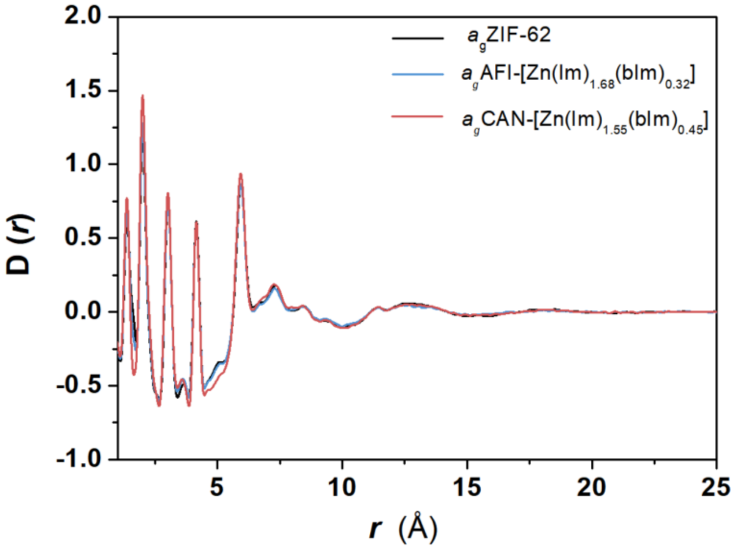

Supplementary Fig. 16 Pair distribution functions, $D(r)$, of a_gAFI-[Zn(Im)$_{1.68}$(bIm)$_{0.32}$], a_gCAN- [Zn(Im)$_{1.55}$(bIm)$_{0.45}$], and a_gZIF-62.

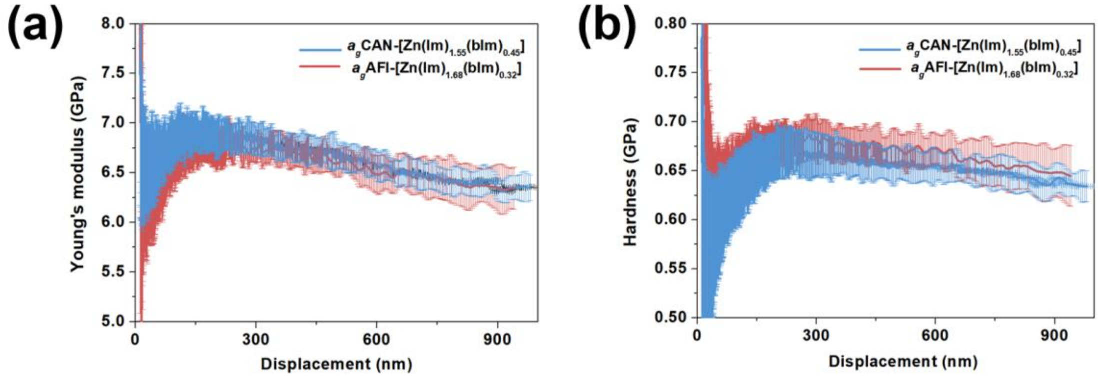

Supplementary Fig. 17 Nano-indentation results of a_gAFI-[Zn(Im)$_{1.68}$(bIm)$_{0.32}$] and a_gCAN- [Zn(Im)$_{1.55}$(bIm)$_{0.45}$]. Error bars represent standard deviations from 5 different analyses.

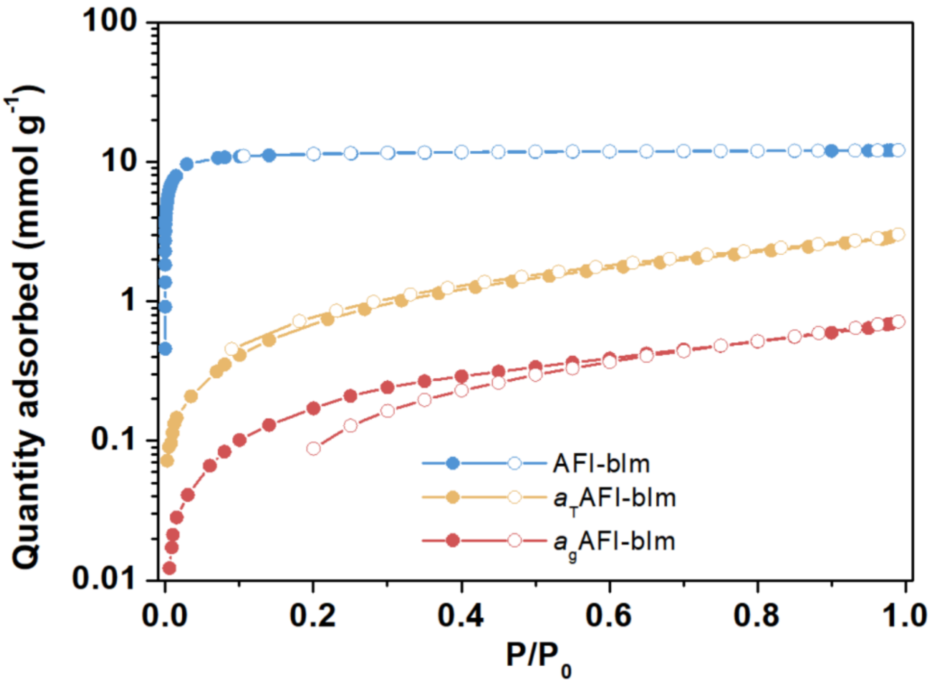

Supplementary Fig. 18 N_2 isotherms of AFI-[Zn(Im)$_{1.68}$(bIm)$_{0.32}$], *a*$_T$AFI-[Zn(Im)$_{1.68}$(bIm)$_{0.32}$], and *a*$_g$AFI-[Zn(Im)$_{1.68}$(bIm)$_{0.32}$] tested at 77 K. The filled and hollow circles represent adsorption and desorption, respectively.

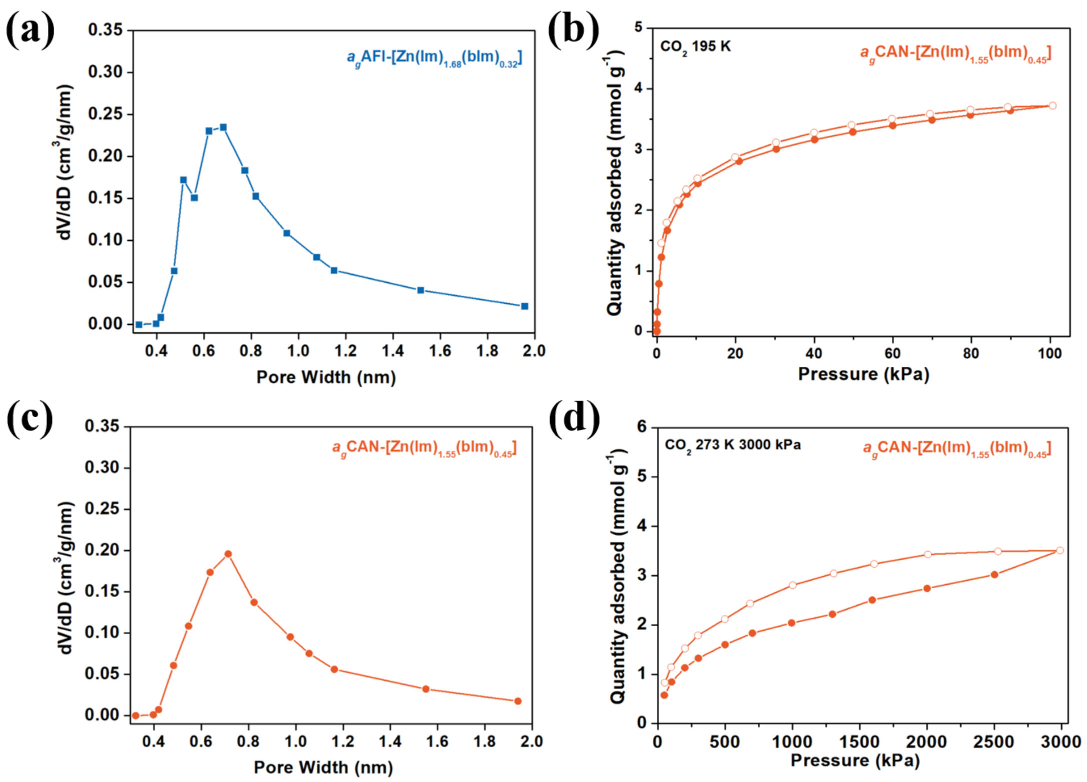

Supplementary Fig. 19 The porosity and pore size distribution of a_gAFI-[Zn(Im)$_{1.68}$(bIm)$_{0.32}$] and a_gCAN-[Zn(Im)$_{1.55}$(bIm)$_{0.45}$]. (a) Pore size distribution of a_gAFI-[Zn(Im)$_{1.68}$(bIm)$_{0.32}$] obtained by CO_2 isotherms at 195 K. (b) CO_2 isotherms at 195K, (c) pore size distribution, and (d) the high-pressure CO_2 adsorption at 273 K and 3000 kPa for a_gCAN-Zn(Im)$_{1.55}$(bIm)$_{0.45}$]. The filled and hollow circles represent adsorption and desorption, respectively.

Supplementary Table 6 Comparison of gas adsorption quantity (mmol g^{-1}) at 100 kPa between a_gAFI-[Zn(Im)$_{1.68}$(bIm)$_{0.32}$] and other MOF glasses and MOF CGCs.

Sample	**Density, g/cm^3**	**H_2, 77 K**	**CO_2, 273 K**	**CH_4, 273 K**	**Ref.**
a_gAFI-[Zn(Im)$_{1.68}$(bIm)$_{0.32}$]	1.381(3)	1.56	1.12	0.45	This work
a_gZIF-62	1.566(1)	0.42	0.89	0.17	S11
a_g[(ZIF-8)$_{0.2}$(ZIF-62)$_{0.8}$]		1.24	0.83	0.21	S11
(MIL-118)$_{0.5}$(a_gZIF-62)$_{0.5}$		1.63	0.49	0.12	S12
(UL-MOF-1)$_{0.5}$(a_gZIF-62)$_{0.5}$		1.53	0.37	0.11	S12

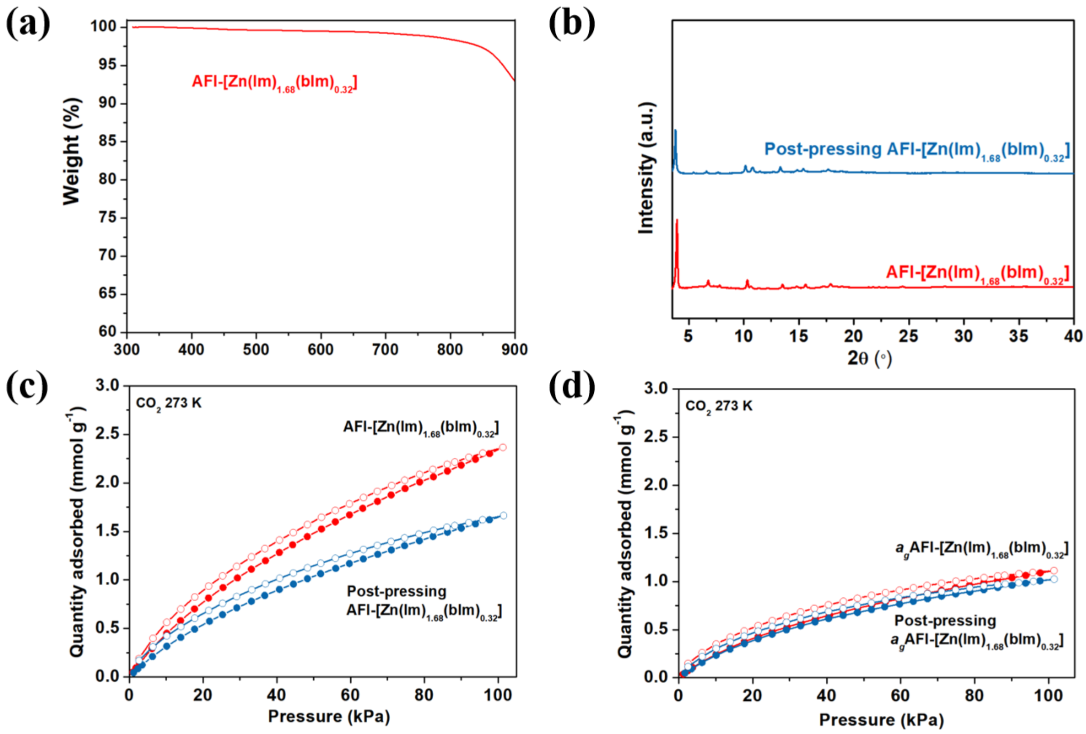

Supplementary Fig. 20 Effects of post-pressing of AFI-[Zn(Im)$_{1.68}$(bIm)$_{0.32}$]. (a) TGA result of AFI-[Zn(Im)$_{1.68}$(bIm)$_{0.32}$] with solvent-free, (b) XRD patterns of post-pressing of AFI-[Zn(Im)$_{1.68}$(bIm)$_{0.32}$], (c) CO_2 adsorption at 273 K for AFI-[Zn(Im)$_{1.68}$(bIm)$_{0.32}$] and post-pressing AFI-[Zn(Im)$_{1.68}$(bIm)$_{0.32}$], (d) CO_2 adsorption at 273 K for a_gAFI-[Zn(Im)$_{1.68}$(bIm)$_{0.32}$] and post-pressing a_gAFI-[Zn(Im)$_{1.68}$(bIm)$_{0.32}$]. The filled and hollow circles represent adsorption and desorption, respectively.

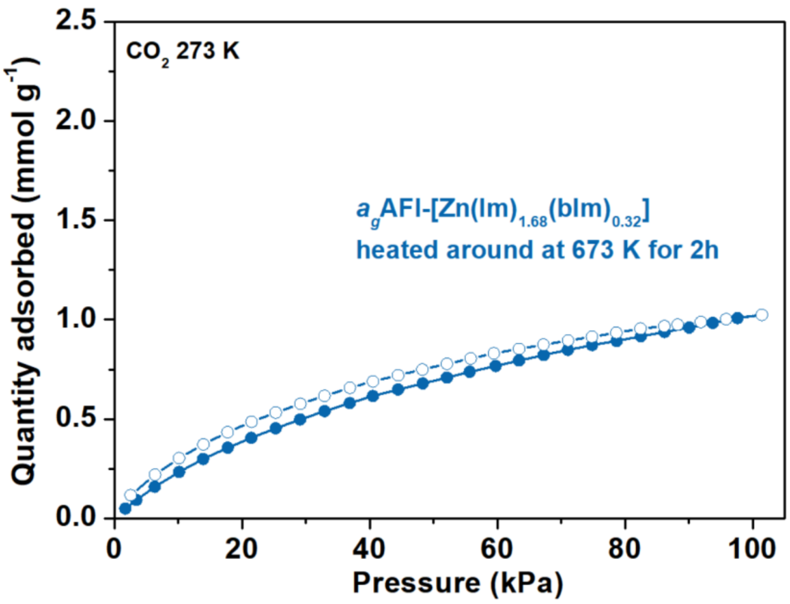

Supplementary Fig. 21 The CO_2 adsorption isotherm of a_gAFI-[Zn(Im)$_{1.68}$(bIm)$_{0.32}$]$_T$ glass heated around at 673 K (above T_g) for 2h.The filled and hollow circles represent adsorption and desorption, respectively.

Supplementary Fig. 22. Cross-sectional SEM images of a_gAFI-[Zn(Im)$_{1.68}$(bIm)$_{0.32}$] membranes with different thicknesses

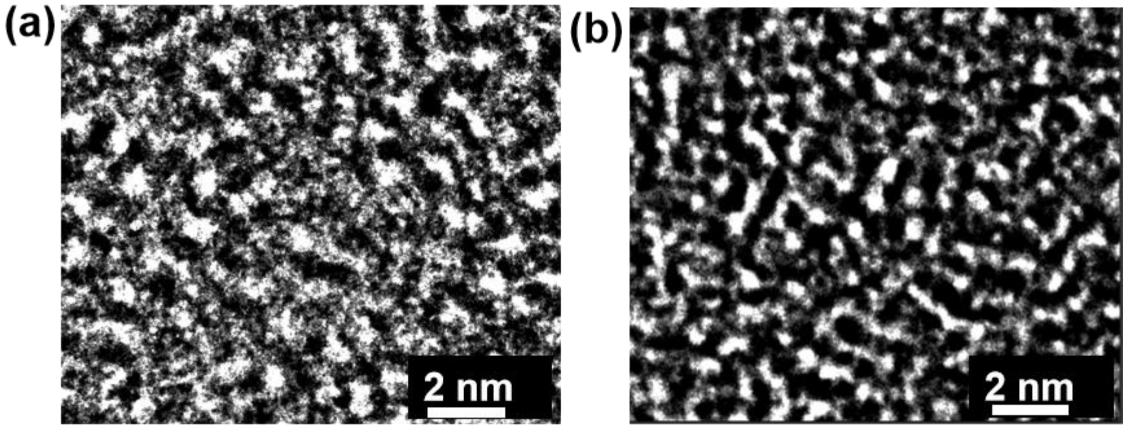

Supplementary Fig. 23. HR-TEM dark field images of (a) a_gZIF-62 membrane, (b) a_gAFI-[Zn(Im)$_{1.68}$(bIm)$_{0.32}$] membrane.

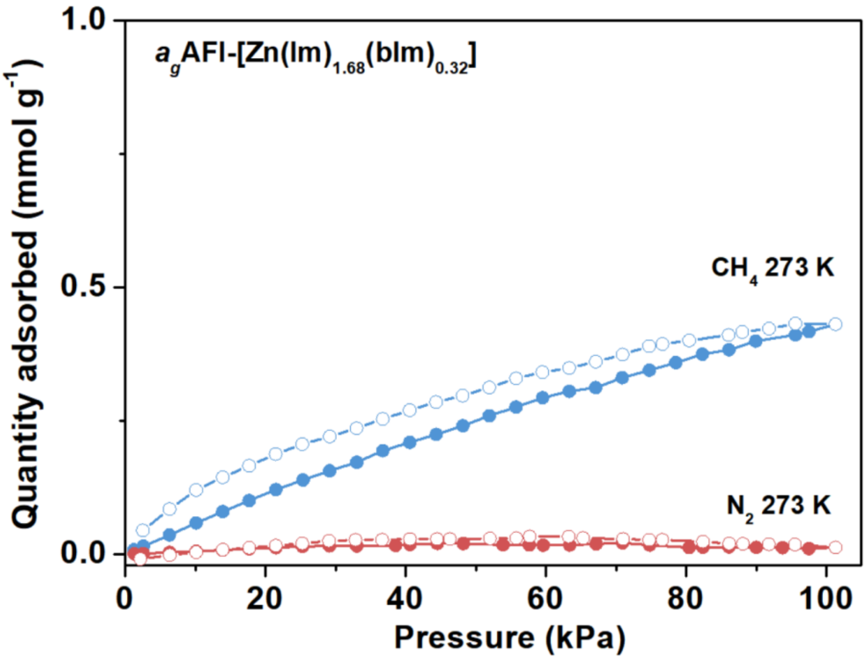

Supplementary Fig. 24 The CH_4 and N_2 adsorption-desorption curves at 273 K for a_gAFI-[Zn(Im)$_{1.68}$(bIm)$_{0.32}$]. The filled and hollow circles represent adsorption and desorption, respectively.

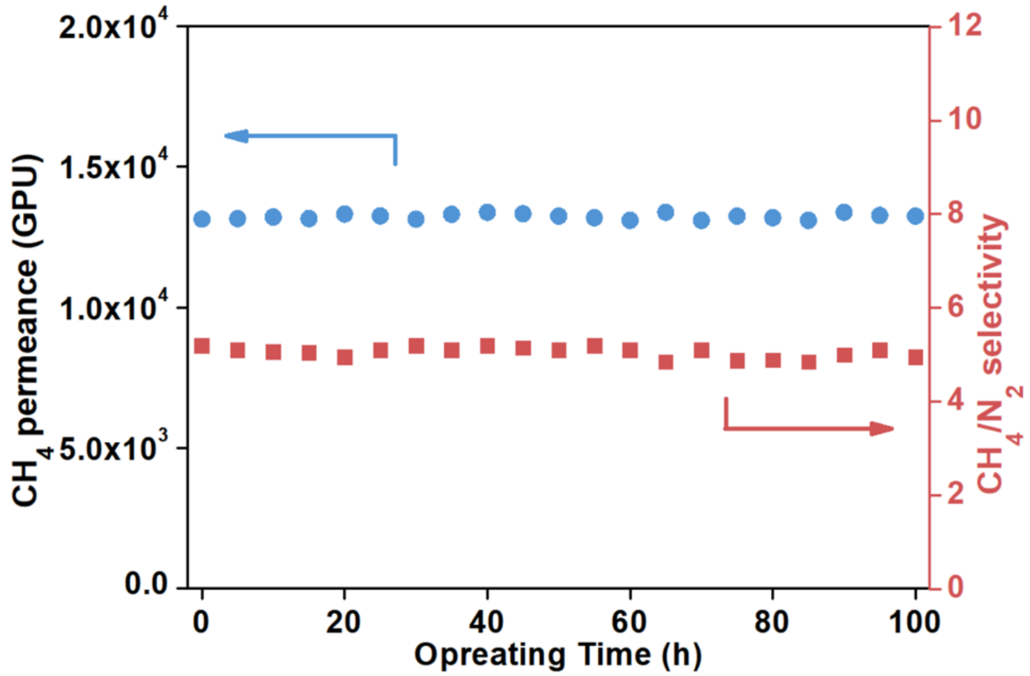

Supplementary Fig. 25. Long-term mixed-gas separation performance of the *a*gAFI-[Zn(Im)1.68(bIm)0.32] membrane (200 µm).

Supplementary Table 7 Separation performance of the a_gAFI-$[Zn(Im)_{1.68}(bIm)_{0.32}]$ and a_gZIF-62 membranes tested by mixed CH_4/N_2 gas.

Membrane	**Thickness (µm)**	**T (K)**	***P* (kPa)**	**R_{CH_4} (GPU)**	***α***
a_gAFI-$[Zn(Im)_{1.68}(bIm)_{0.32}]$	~ 100	298	50	15524	3.8
a_gAFI-$[Zn(Im)_{1.68}(bIm)_{0.32}]$	~ 200	298	50	13260	5.2
a_gAFI-$[Zn(Im)_{1.68}(bIm)_{0.32}]$	~ 300	298	50	10400	6.4
a_gZIF-62	~ 200	298	50	44.6	1.2

Supplementary Table 8. Gas permeability, solubility coefficient and diffusivity coefficient of the a_gAFI-[Zn(Im)$_{1.68}$(bIm)$_{0.32}$] and a_gZIF-62 membranes (~200 μm).

Membrane	CH_4 permeability [10^3 barrer]	Solubility coefficient [10^{-3} cm^3/(cm^3 cmHg)]		S_{CH_4/N_2}	Diffusivity coefficient [10^{-4} cm^2/s]		D_{CH_4/N_2}
		CH_4	N_2		CH_4	N_2	
a_gAFI-[Zn(Im)$_{1.68}$(bIm)$_{0.32}$]	3238	70.28	12.59	5.58	46.07	42.16	1.09
a_gZIF-62	14	25.53	9.71	2.63	0.56	1.05	0.53

Supplementary Table 9. Gas permeability, solubility coefficient and diffusivity coefficient of the a_gAFI-[Zn(Im)$_{1.68}$(bIm)$_{0.32}$] and a_gZIF-62 membranes (~200 μm).

Membrane	CO_2 permeability [10^3 barrer]	Solubility coefficient [10^{-3} cm^3/(cm^3 cmHg)]		S_{CO_2/N_2}	Diffusivity coefficient [10^{-4} cm^2/s]		D_{CO_2/N_2}
		CO_2	N_2		CO_2	N_2	
a_gAFI-[Zn(Im)$_{1.68}$(bIm)$_{0.32}$]	10350	113.40	12.75	8.89	91.33	42.18	2.16
a_gZIF-62	61	27.54	9.43	2.92	2.88	1.01	2.85

Supplementary Table 10. Gas separation performance comparison of the a_gAFI-[Zn(Im)$_{1.68}$(bIm)$_{0.32}$] membrane with other reported membranes having high performance for CO_2/N_2 separation.

Symbol	**Membrane**	P_{CO_2} **(GPU)**	α	**Ref.**
▲	UIO-66/AAO	2070	34.7	S13
●	MIL-100/AAO	2700	3.8	S14
▲	ZIF-8/GO/AAO	102	7	S15
▼	CAU-1/AAO	4080	14.8	S16
⬟	Co/Zn-ZIF-L	175.8	16	S17
◀	UiO-66 (TG)/AAO	1221	27.6	S18
▶	MIL-160/AAO	508.2	33.3	S19
⬢	ZIF-7/PSf hollow fiber	2.7	11.7	S20
⬢	PTO-30/TFC-MMM	1828	32	S21
⬟	TFC_PEBA(10IL)_ZIF94(15)	819	25	S22
◆	HPEO2-800/PDMS/PSF membrane	850	37	S23
◆	MOF-5/PI	0.267	14.16	S24
■	AZIF-8/PI	32	20.5	S25
▲	B-PIM-1	3100	19	S26
◆	UIO-66/PIM	79	21	S27
■	MOF-801/PIM	215	27	S28
⬢	a_gZIF-62/AAO	37	34	S29
▲	a_gTIF-4/AAO	21	27	S30
★	a_gZIF-62	305	8.3	This work
☆	a_gAFI-[Zn(Im)$_{1.68}$(bIm)$_{0.32}$]	51753	19.5	This work
★	a_gAFI-[Zn(Im)$_{1.68}$(bIm)$_{0.32}$]	37485	14.8	This work

Supplementary Table 11. Gas separation performance comparison of CH_4/N_2 separation performance of the a_gAFI-[Zn(Im)$_{1.68}$(bIm)$_{0.32}$] membranes with other reported membranes having high performance for CH_4/N_2 separation.

Symbol	**Membrane**	P_{CH4} **(GPU)**	α	**Ref.**
■	[Ni$_3$(HCOO)$_6$]/SBS-5	1.23	3.1	S31
●	Ni-MOF-74/SBS-15	0.83	2.94	S32
▲	SBS10SN	0.28	7.2	S33
▷	PVAm-CACl-10 (180)/MPSf	447	2.28	S34
◆	PAA/ZIF-8@VR800	1763	3.12	S35
●	ZIF-62-L/PEI	2276	3.96	S36
◓	PVA/ACU-120A/MPSf	5584	3.43	S37
⬘	PVAm/CSZ/MPSf	7600	4.35	S38
▲	Single crystal ZIF-8	0.26	3.6	S39
◀	TPC-RCC3@PIP/mPSf	1216	3	S40
▼	CNT/PES membrane	1158	1.7	S41
◀	a_{gf}ZIF-62	45000	4.34	S42
★	a_gZIF-62	44.6	1.2	This work
☆	a_gAFI-[Zn(Im)$_{1.68}$(bIm)$_{0.32}$]	16189	6.1	This work
★	a_gAFI-[Zn(Im)$_{1.68}$(bIm)$_{0.32}$]	13260	5.2	This work

Reference:

[S1] Bumstead A M, Gómez M L R, Thorne M F, et al. Investigating the melting behaviour of polymorphic zeolitic imidazolate frameworks[J]. *Cryst. Eng. Comm.*, 22(21) (2020) 3627-3637.

[S2] Lai Z. Development of ZIF-8 membranes: opportunities and challenges for commercial applications[J]. *Curr. Opin. Chem. Eng.*, 20 (2018) 78-85.

[S3] Gandara-Loe J, Bueno-Perez R, Missyul A, Fairen-Jimenez D, Silvestre-Albero J. Molecular Sieving Properties of Nanoporous Mixed-Linker ZIF-62: Associated Structural Changes upon Gas Adsorption Application. *ACS Appl. Nano. Mater.* **4**, (2021) 3519-3528.

[S4] Bennett T D, Yue Y, Li P, et al. Melt-quenched glasses of metal–organic frameworks. *J. Am. Chem. Soc.*, 138(10) (2016) 3484-3492.

[S5] Anh Phan, Christian J. Doonan, Fernando J. Uribe-Romo, Carolyn B. Knobler, Michael O'Keeffe, Omar M. Yaghi, Synthesis, Structure, and Carbon Dioxide Capture Properties of Zeolitic Imidazolate Frameworks, *Acc. Chem. Res.* 43 (2010) 58-67.

[S6] Qi Shi, Wei-Jian Xu, Rui-Kang Huang, Wei-Xiong Zhang, Yang Li, Pengfei Wang, Fa-Nian Shi, Libo Li, Jinping Li, Jinxiang Dong, Zeolite CAN and AFI-Type Zeolitic Imidazolate Frameworks with Large 12-Membered Ring Pore Openings Synthesized Using Bulky Amides as Structure-Directing Agents, *J. Am. Chem. Soc.* 138 (2016) 16232-16235.

[S7]. Qiao A, et al. A metal-organic framework with ultrahigh glass-forming ability. Sci. Adv. **4**, eaao6827 (2018).

[S8]. Frentzel-Beyme L, Kolodzeiski P, Weiß J-B, Schneemann A, Henke S. Quantification of gas accessible microporosity in metal-organic framework glasses. Nat. Commun. **13**, 7750 (2022).

[S9]. Bumstead, A. M. et al. Investigating the melting behaviour of polymorphic zeolitic imidazolate frameworks. CrystEngComm **22**, 3627–3637 (2020).

[S10]. Xue WL, et al. Highly porous metal–organic framework liquids and glasses via a solvent-assisted linker exchange strategy of ZIF–8. Nat Commun. 15, 4420 (2024).

[S11] Longley L, *et al.* Flux melting of metal–organic frameworks. *Chem Sci* **10**, 3592 3601 (2019).

[S12] Ashling CW, *et al.* Guest size limitation in metal–organic framework crystal–

glass composites. *J Mater Chem A* **9**, 8386-8393 (2021).
[S13] Y.W. Sun, J.H. Yan, Y.L. Gao, T.T. Ji, S.X. Chen, C. Wang, P. Lu, Y.S. Li, Y. Liu, Fabrication of Highly Oriented Ultrathin Zirconium Metal-Organic Framework Membrane from Nanosheets towards Unprecedented Gas Separation, Angew. Chem. Int. Ed. 62 (2023) e202216697.
[S14] Z.S. Dou, J.F. Cai, Y.J. Cui, J.C. Yu, T.F. Xia, Y. Yang, G.D. Qian, Preparation and Gas Separation Properties of Metal-Organic Framework Membranes, Anorg. Allg. Chem. 641 (2015) 792-796.
[S15] Y.X. Hu, J. Wei, Y. Liang, H.C. Zhang, X.W. Zhang, W. Shen, H.T. Wang, Zeolitic Imidazolate Framework/Graphene Oxide Hybrid Nanosheets as Seeds for the Growth of Ultrathin Molecular Sieving Membranes, Angew. Chem. Int. Ed. 5 (2016) 2048-2052.
[S16] Y. Jian, H. Yin, F. Chang, L. Cheng, J. Yang, W. Mu, X. Li, J. Lu, Y. Zhang, J. Wang, Facile synthesis of highly permeable CAU-1 tubular membranes for separation of CO_2/N_2 mixtures, J. Membr. Sci. 522 (2017) 140-150.
[S17] J.Y. Zhu, H. Li, J.W. Hou, J.D. Liu, Y.T. Zhang, B.V. Bruggen, Heteroepitaxial growth of vertically orientated zeolitic imidazolate framework-L (Co/Zn-ZIF-L) molecular sieve membranes, AlChE J. 66 (2020) e16935.
[S18] J.H. Yan, Y.W. Sun, T.T. Ji, L.L. Liu, M. Zhang, Y. Liu, Cooperative defect tailoring: A promising protocol for exceeding performance limits of state-of-the-art MOF membranes, J. Membr. Sci. 635 (2021) 119515.
[S19] W. Fan, Y. Ying, S.B. Peh, H. Yuan, Z. Yang, Y.D. Yuan, D. Shi, X. Yu, C. Kang, D. Zhao, Multivariate Polycrystalline Metal-Organic Framework Membranes for CO_2/CH_4 Separation, J. Am. Chem. Soc. 143 (2021) 17716-17723.
[S20] F. Cacho-Bailo, S. Catalán-Aguirre, M. Etxeberría-Benavides, O. Karvan, V. Sebastian, C. Téllez, J. Coronas, Metal-organic framework membranes on the inner-side of a polymeric hollow fiber by microfluidic synthesis, J. Membr. Sci. 476 (2015) 277-285.
[S21] H.J. Min, M. Kang, Y.S. Bae, R. Blom, C.A. Grande, J.H. Kim, Thin-film composite mixed-matrix membrane with irregular micron-sized UTSA-16 for outstanding gas separation performance, J. Membr. Sci. 669 (2023) 121295.
[S22] L. Martínez-Izquierdo, C. Téllez, J. Coronas, Highly stable Pebax® Renew® thin-film nanocomposite membranes with metal-organic framework ZIF-94 and ionic liquid [Bmim][BF_4] for CO_2 capture, J. Mater. Chem. A, 10 (2022) 18822.

[S23] G.Y. Zhang, T.N. Tran, L. Huang, E. Deng, A. Blevins, W.J. Guo, Y.F. Ding, H.Q. Lin, Thin-film composite membranes based on hyperbranched poly(ethyleneoxide) for CO_2/N_2 separation, J. Membr. Sci. 644 (2022) 120184.

[S24] H.Q. Ren, J.Y. Jin, J. Hu, H.L. Liu, Affinity between Metal-Organic Frameworks and Polyimides in Asymmetric Mixed Matrix Membranes for Gas Separations, Ind. Eng. Chem. Res. 51(30) (2012) 10156-10164.

[S25] H. An, K.Y. Cho, Q. Lyu, D.S. Chiou, K.J. Nam, D.Y. Kang, L.C. Lin, J.S. Lee, Facile Defect Engineering of Zeolitic Imidazolate Frameworks towards Enhanced C_3H_6/C_3H_8 Separation Performance, Adv. Funct. Mater. 31 (2021) 2105577.

[S26] M. Yu, A.B. Foster, M. Alshurafa, J.M. Luque-Alled, P. Gorgojo, S.E. Kentish, C.A. Scholes, P.M. Budd, CO_2 separation using thin film composite membranes of acid-hydrolyzed PIM-1, J. Membr. Sci. 679 (2023) 121697.

[S27] C.X. Geng, Y.X. Sun, Z.Q. Zhang, Z.H. Qiao, C.L. Zhong, Mitigated Aging in a Defective Metal-Organic Framework Pillared Polymer of an Intrinsic Porosity Hybrid Membrane for Efficient Gas Separation, ACS Sustainable Chem. Eng. 10 (2022) 3643-3650.

[S28] W.B. Chen, Z.G. Zhang, L. Hou, C.C. Yang, H.C. Shen, K. Yang, Z. Wang, Metal-organic framework MOF-801/PIM-1 mixed-matrix membranes for enhanced CO_2/N_2 separation performance, Sep. Purif. Technol. 250 (2020) 117198.

[S29] H.N. Xia, H. Jin, Y.T. Zhang, H. Song, J.Q. Hu, Y. Huang, Y.S. Li, A long-lasting TIF-4 MOF glass membrane for selective CO_2 separation, J. Membr. Sci. 655 (2022) 120611.

[S30] Y.H. Wang, H. Jin, Q. Ma, K. Mo, H.Z. Mao, A. Feldhoff, X.Z. Cao, Y.S. Li, F.S. Pan, Z.Y. Jiang, A MOF Glass Membrane for Gas Separation, Angew. Chem. Int. Ed. 590 (2020) 4365-4369.

[S31] S.M. Wang, Q.P. Guo, S.J. Liang, P. Li, X. Li, X. J.J. Luo, $[Ni_3(HCOO)_6]$/Poly(styrene-b-butadiene-b-styrene) mixed-matrix membranes for CH_4/N_2 gas separation, Chem. Eng. Technol. 41 (2) (2018) 353-366.

[S32] S.M. Wang, Q.P. Guo, S.J. Liang, P. Li, J.J. Luo, Preparation of Ni-MOF-74/SBS mixed matrix membranes and its application of CH_4/N_2 separation, Sep. Purif. Technol. 199 (2018) 206-213.

[S33] P.P. Guan, J.J. Luo, W. Li, Z.Q. Si, Enhancement of gas permeability for CH_4/N_2 separation membranes by blending SBS to Pebax polymers, Macromol. Res. 2017, 25 (10) 1007-1014.

[S34] L. Guan, Z.J. Ma, X.Y. Guo, Z.H. Qiao, C.L. Zhong, Transforming 3D CAU-10-H into 2D Materials with High Base Stability for Membrane Separation, Chem. Asian. J. 16 (2021) 1-9.

[S35] Z.J. Gu, Z.B. Yang, X.Y. Guo, Z.H. Qiao, C.L. Zhong, Vacuum resistance treated ZIF-8 mixed matrix membrane for effective CH_4/N_2 separation, Sep. Purif. Technol. 272 (2021) 118845.

[S36] C. Ma, Z.B. Yang, X.Y. Guo, Z.H. Qiao, C.L. Zhong, Size-reduced low-crystallinity ZIF-62 for the preparation of mixed-matrix membranes for CH_4/N_2 separation, J. Membr. Sci. 663 (2022) 121069.

[S37] Z.J. Yu, Z.J. Gu, J.B. Lei, G. Zheng, Vacuum treated amorphous MOF mixed matrix membrane for methane/nitrogen separation, J. Solid State Chem. 320 (2023) 123852.

[S38] Z.J. Gu, Z.B. Yang, Y.X. Sun, Z.H. Qiao, C.L. Zhong, Large-area vacuum-treated ZIF-8 mixed-matrix membrane for highly efficient methane/nitrogen separation, AIChE J. 68 (2022) e17749.

[S39] C. Chen, A. Ozcan, A.O. Yazaydin, B.P. Ladewig, Gas permeation through single-crystal ZIF-8 membranes, J. Membr. Sci. 575 (2019) 209-216.

[S40] Z.H. Jiang, Y. Wang, M.L. Sheng, Z.Y. Zha, J.X. Wang, Z. Wang, S. Zhao, A highly permeable porous organic cage composite membrane for gas separation, J. Mater. Chem. A 11 (2023) 6831-6841.

[S41] Samy Yousef, Simona Tuckute, Andrius Tonkonogovas, Arūnas Stankevičius, Alaa Mohamed, Ultra-permeable CNTs/PES membranes with a very low CNTs content and high H_2/N_2 and CH_4/N_2 selectivity for clean energy extraction applications, J. Mater. Res. Technol. 15 (2021) 5114-5127.

[S42] Z.B. Yang, Y. Belmabkhout, L.N. McHugh, D. Ao, Y.X. Sun, S.C. Li, Z.H. Qiao, T.D. Bennett, M. D. Guiver, C.L. Zhong. ZIF-62 glass foam self-supported membranes to address CH_4/N_2 separations. Nat. Mater. 22(7) (2023) 888.